Journal of Applied Polymer Science

Structure and Dielectric Breakdown Strength of Nano Calcium Carbonate/Polypropylene Composites

Suvi Virtanen,[1] Hannes Ranta,[2] Susanna Ahonen,[1] Mikko Karttunen,[3] Jani Pelto,[3] Kari Kannus,[2] Mika Pettersson[1]

[1]Nanoscience Center, Department of Chemistry, P.O. Box 35, FI-40014 University of Jyväskylä, Jyväskylä, Finland
[2]Department of Electrical Energy Engineering, Tampere University of Technology, P.O. Box 692, 33101 Tampere, Finland
[3]Technical Research Centre of Finland, P.O. Box 1607, 33101 Tampere, Finland
Correspondence to: S. Virtanen (E-mail: suvi.t.h.virtanen@jyu.fi)

ABSTRACT: Nanodielectrics, a 21st-century phenomena, is envisioned to be the answer for material challenges in progressive high-voltage technology. It is well known that the proper dispersion of nanoparticles plays a key role in improving the dielectric properties of a material, but to understand where changes in the properties of a material originate, it is also essential to reveal the multiscale structure of the material. In this study, the dielectric permittivity, breakdown strength, and structure of nano calcium carbonate (nano-$CaCO_3$)/polypropylene composites with 1.8–8.1 wt % doping were characterized systematically. The combined results from transmission electron microscopy, Raman microscopy, and optical microscopy show that the quality of nanodispersion was similar in all of the filler concentrations studied. However, all of the samples also contained smoothly distributed microparticles. The density of the microparticles increased exponentially when the concentration of nano-$CaCO_3$ was increased in the manufacturing process. The dielectric direct-current breakdown of the composites had a maximum at 1.8 wt % concentration and then decreased as the filler concentration was increased. The differences could be explained by the existence of large microparticles rather than the quality of the nanoparticle dispersion; this indicated the importance of multiscale characterization. © 2013 Wiley Periodicals, Inc. J. Appl. Polym. Sci. **2013**, *131*, 39504.

KEYWORDS: composites; dielectric properties; microscopy; spectroscopy; structure; property relations

Received 13 June 2012; accepted 3 May 2013
DOI: 10.1002/app.39504

INTRODUCTION

The concept of nanodielectrics means dielectric materials that are doped with small mass amounts of inorganic particles with sizes of 1–100 nm to produce a large interfacial area between the matrix polymer and the nanofillers and hence alter the dielectric properties.[1] The nanoparticles are used in both crosslinked thermosetting polymers and in semicrystalline thermoplastics. In particular, in the use of thermoplastics that are recyclable, it is possible to achieve more applicable and economical insulation structures.[2] However, the heterogeneous nature of the composition of these polymer nanocomposites brings challenges and requirements to the development of the processing methods.[3] Also, quite high filler loadings close to percolation threshold, such as 10 wt % for epoxy TiO_2, were reported to be optimal for gaining a good dielectric breakdown strength.[4] To develop these new materials for industrial use, a fundamental understanding of the dielectric properties at the nanoscale level is of great importance.[5] Previously, it was shown that around each nanoparticle there is a region with enhanced local conductivity that provides a mechanism for the redistribution of charge around the particle; this increases the voltage endurance of the composites.[6] For example, a promising hundredfold improvement in treeing resistance was achieved in a 5 wt % SiO_2 crosslinked polyethylene composite useful for cable applications. For this particular material, it has been shown that the degree of crystallinity is not a predominant factor in increasing the breakdown strength and that the highest voltage endurance occurs for composites with strong covalent bonding between the matrix and the filler.[7] Especially high interest in this field has been devoted to the possibility of using these new type of materials in capacitor applications.[8,9]

Calcium carbonate ($CaCO_3$) has commonly been used in large mixture ratios to reinforce polypropylene (PP).[10] The problem for dielectric studies of $CaCO_3$-filled polymer composites has

Additional Supporting Information may be found in the online version of this article.

been the effect of absorbed moisture.[11] For $CaCO_3$-filled PP composites, a raised alternating-current (ac) breakdown strength was reported.[12] The effect of nano calcium carbonate (nano-$CaCO_3$) on the mechanical properties of PP has been studied with various approaches.[13–16]

To elucidate the relationship between the structure and the dielectric properties, it is useful to study the structure of the material both at the microscale and the nanoscale. For possible applications, it is also important to understand the detailed composition of the material to avoid possible drawbacks caused by large microparticles formed by the agglomeration of nanoparticles.

In this study, we concentrated on the systematic structural characterization of nano-$CaCO_3$/PP composites manufactured by twin-screw extrusion followed by biaxial orientation. The structure of the composites was studied both at the nanoscale and the microscale to reveal the effects of changes in the concentration of the filler particles on the multiscale structure of the material. Dielectric spectroscopy was used to obtain insight into the dielectric nature of the materials. The dielectric breakdown strength measurements were carried out for the same samples to establish a correlation between the structure and dielectric breakdown strength.

EXPERIMENTAL

Materials

Borealis HC318BF PP homopolymer, 1.8–8.1 wt % stearic acid treated Socal 322 precipitated $CaCO_3$ (Solvay), and 0.05–0.1 wt % antioxidants were first mechanically dry-mixed and subsequently melt-mixed in a Berstorff ZE25/43D corotating twin-screw extruder. The screw geometry consisted of two kneading sections. The melt was vacuum degassed after the second kneading section. The extruder was purged with 5 L/min nitrogen gas during the compounding. An amount of 3.5 kg/h of the dry-mixed material was fed into the extruder gravimetrically. The extruder temperature set point was 190°C. The melting temperature (205–210°C) was measured after the second kneading section. The extruder speed was set at 300 rpm. The compounded material was air-cooled on a steel conveyor belt in a dust-free environment and pelletized with a strand cutter.

The nano-$CaCO_3$/PP compound was extruded through a custom-made, 120-mm slot die attached to a Brabender PL2100-6 plasticorder equipped with an Extrusiongraph 19/25D single-screw extruder (3/1 screw) in a controlled, dust-free environment. The extruder speed was set at 100 rpm. The melting temperature varied between 215 and 235°C, and the cast film thickness varied from 700 to 500 μm, respectively. The melt was cast onto a chill roll at 90°C to avoid orientation of the molten polymer. The cast PP films were biaxially stretched to a fixed 5.6 × 5.6 draw ratio (100 s, with preheating at 155–160°C and a 100% drawing rate) with a Bruckner KARO IV system. The oriented 20–25 μm thick films were protected from UV exposure and stored several days before electrical testing.

Methods

Structural Characterization. The analysis was done for PP composite sample series containing 1.8–8.1 wt % nano-$CaCO_3$. Altogether, there were samples of eight different nano-$CaCO_3$ concentrations. Pure PP, processed similarly as the composites, was used as a reference. Both cast and oriented film samples were characterized. For transmission electron microscopy (TEM) analysis, ultrathin sections of the cast film sample were obtained with a Diatome 45° diamond knife at room temperature with a Leica Reichert Ultracut ultramicrotome. The approximately 90 nm thick sections were collected on a 400-mesh copper grid and imaged with a JEOL JEM-1200EX electron microscope with 2500–15,000 magnification. The statistical analysis was made from images that were converted to binary format. The particle area and the center of mass were determined with the ImageJ program. Microparticles were excluded from this analysis. The data was further processed to emphasize the distribution of the filler material in the matrix media; the relative volume of the agglomerates was estimated with the assumption that they were spherical objects. The dispersion was quantified with the nearest neighbor index (NNI) and skewness of the distribution after the particles in quadrats.[17] When counting particles in quadrats, we selected the size of the quadrat to be two times the average diameter of the agglomerates, as is common.[18]

For the Raman analysis of the cast film samples, a dispersive micro-Raman spectrometer (Bruker Senterra R200–785) equipped with a linearly polarized diode laser (785 nm) was used. The laser power was 100 mW, and a slit width of 50 × 1000 μm^2 was used with a 50× objective to get a good signal. The area of interest in the sample was scanned with a motorized stage with 0.1 μm accuracy in two dimensions with a 3 μm step size. The spectra of the composites were measured from a 210 × 210 μm^2 area. Four areas of each sample were scanned and visualized as an intensity contour plot of a selected characteristic Raman peak of $CaCO_3$ or PP. The PP signal was used as a reference to check that the overall signal level was stable over the measured area. The microparticle distribution was quantified over a large area to get a better idea of the particle dispersion in the scale corresponding to the electrode area used in the dielectric breakdown strength measurements. Microparticles with a size greater than 2 μm were counted manually by inspection of the oriented samples with an optical microscope. It was first confirmed by Raman measurements that the particles consisted of $CaCO_3$. The dispersion at the microscale was quantified with NNI and by a method that was analogous to determining the skewness of the distribution after the particles in quadrats were counted,[17] but in this case, 60 quadrats altogether with a size of 130 × 100 μm^2 were arbitrarily distributed in three 6 cm^2 areas that were randomly selected from a 200-cm^2 oriented film sample. It was also notable that the particle size varied significantly; particles even up to 60 μm were present. The total analyzed area for each sample was 0.78 mm^2.

Dielectric Characterization. The dielectric direct-current (dc) breakdown strengths of a total of 20 parallel samples per 1 biaxially oriented sample were measured. The test voltage, a steadily rising dc ramp of 400 V/s, was applied to each sample by cylindrical steel rod electrodes with an approximate total area of 1 cm^2 with graphite plates in between. The electrode setup was immersed in transformer oil (Shell Diala DX). The thickness of

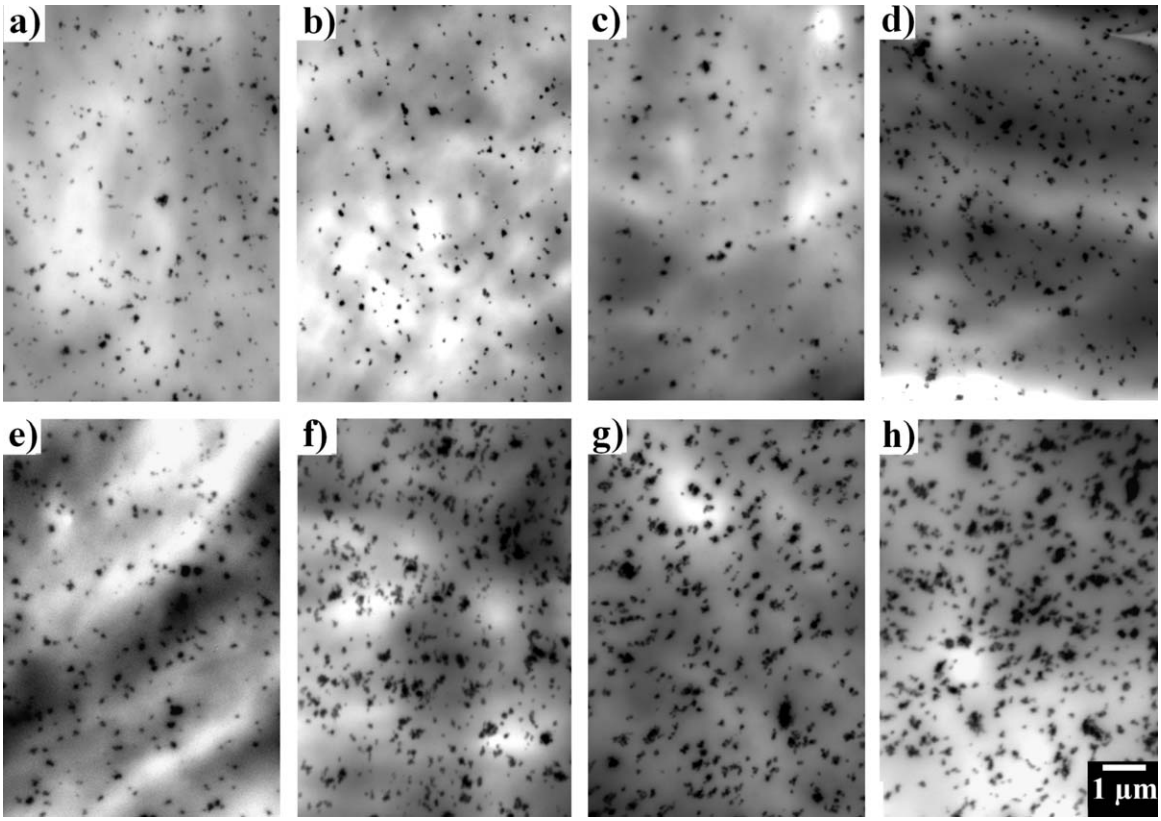

Figure 1. TEM images of the (a) 1.8, (b) 2.7, (c) 3.6, (d) 4.6, (e) 5.6, (f) 6.4, (g) 7.4, and (h) 8.1 wt % nano-$CaCO_3$/PP composite samples.

each sample was measured with a micrometer before the test. The breakdown results were fitted into a two-parameter Weibull distribution, whose cumulative distribution function is given by

$$F(x)=1-\exp\left\{-\left(\frac{x}{\alpha}\right)^{\beta}\right\}. \quad (1)$$

where $F(x)$ is the probability of breakdown at an electric field strength of x (V/μm). The scale parameter (α) is related to the 63.2% probability of breakdown at field strength, and the shape parameter (β) describes the shape of the distribution; the higher the value of β is, the narrower the spread of individual breakdown strength results. The adequacy of the Weibull distribution was checked, and 90% confidence bounds were calculated.[19]

Dielectric spectroscopy was done for the cast film samples, sized as 9 × 9 cm^2, on which circular aluminum foil electrodes of Ø = 8 cm were applied with a small amount of silicon grease.[21] Three parallel samples were tested for each composite. The effective thickness of each sample was determined with a micrometer as an 18-measurement average from the electrode area. Three consecutive measurements were conducted for each sample, with a total of nine measurements added up per material. The complex impedance of the samples was measured with an insulation diagnostics analyzer (IDA 200) at an ac measuring voltage of 140 V_{RMS} and a frequency range from 0.01 Hz to 1 kHz. The ambient temperature and relative air humidity during the measurements varied from 19.5 to 21.1°C and from 34 to 40%, respectively. The real and imaginary parts of the complex permittivity (ε' and ε'' respectively) were calculated from the measured parallel capacitance and resistance according to eqs. (2) and (3):

$$\varepsilon'=\left(\frac{C_P-C_e}{C_0}\right), C_0=\frac{\varepsilon_0 A}{d} \quad (2)$$

$$\varepsilon''=\varepsilon'\tan\delta=\frac{\varepsilon'}{2\pi R_P C_P f} \quad (3)$$

where C_P and R_P are the measured parallel capacitance and resistance, respectively, at a frequency of f; C_e is the error capacitance due to small electric field distortion at the electrode edges;[21] C_0 is the vacuum (geometric) capacitance defined by the electrode area (A), the permittivity of the vacuum (ε_0), and the average thickness of the sample (d); and tan δ is the dielectric loss tangent.

RESULTS AND DISCUSSION

Structural Characterization

Nanoparticles. Figure 1 shows representative TEM images taken of the cast film samples. It was evident that in all of the composites there were particles dispersed at the nanoscale. Quantitative analysis of several images from random places in every sample was done, and it showed that the mean diameter of these agglomerates grew approximately linearly when the weight percentage was increased in the composite samples. (see Figure 2). From histograms showing the distribution of $CaCO_3$ nanoparticles in each cast film sample, we observed that the distribution

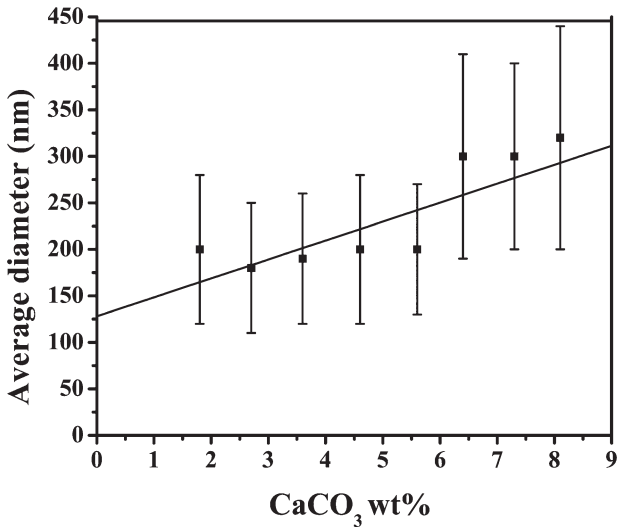

Figure 2. Average nanoparticle diameter in the composites determined from the relative volume of the $CaCO_3$ agglomerates.

flattened, broadened, and shifted as the concentration of nano-$CaCO_3$ increased in the composite material (see Figure 1 in the Supporting Information). The dispersion could be considered smooth for all of the samples because NNI was above 1 and the skewness was relatively close to zero regardless of the doping level (Figure 9, shown later). These values fell into a range that could be associated with good mixing and a regularity of the dispersion.[17,18] During this analysis, systematic data from the microparticles was not gathered, but we noticed that abundant microparticles made it difficult to obtain good-quality ultrathin sections from the cast films because the particles were much harder than the matrix PP. The PP matrix itself was used as a reference to monitor the structure alteration during the sectioning of the composites. We could easily see from the PP microcrystal structure whether there were any distortions in the section area.

Microparticles. Optical microscope images from selected oriented film samples are shown in Figure 3. As shown, the microstructure of PP changed dramatically when $CaCO_3$ was introduced, as reported previously.[13] The in-depth statistical analysis of the oriented composite samples showed that the microparticle density increased exponentially as the amount of nano-$CaCO_3$ was increased, as shown in Figure 4(a). Even at the lowest concentration of 1.8 wt %, the density of microparticles was on the order of hundreds per square millimeter; this would be very significant, for example, for capacitor applications. At the nanoscale, such samples appeared to contain a smooth nanodispersion, as shown in Figure 1(a). The value for NNI was above 1, and the skewness value of the distribution after the microparticles were counted in randomly distributed quadrats was relatively close to 0; this indicated that in the scale proportional to the area used in the dielectric breakdown strength measurements, the microparticle distribution was smooth. Thus, in all of the samples, there were microparticles present in the measurement area. When the studied scale was smaller, the distribution of microparticles could be considered smooth only at higher filler concentrations. From histograms showing the distribution of $CaCO_3$ microparticles counted in randomly distributed quadrats for each oriented sample, we observed that the distribution flattened, broadened, and shifted as the concentration of nano-$CaCO_3$ increased in the composite material (see Figure 2 in the Supporting Information).

The microparticles with sizes over 10 μm were counted separately, and their amount also grew exponentially as the filler content increased [see Figure 4(b)]. Large particles are problematic because when the particle size approaches the film thickness, they become severely destructive for most applications because of the formation of holes during the stretching in the biaxial orientation stage.[10] There were only a few such particles per square millimeter in the samples with the lowest concentrations, as shown in Figure 4(b). Overall, the results show that although the quality of the nanodispersion was smooth throughout the whole concentration range studied, the amount of microparticles increased dramatically as the concentration was increased. Qualitatively, we deduced that through the addition of more filler material, the main effect was to grow large microparticles, whereas the average size of the nanoparticles increased relatively slowly. As the added material accumulated in large particles, the effective nanoparticle concentration and size did not change so dramatically. As the presence of large particles is mostly considered harmful, it is evident that in thin-film applications, it would be beneficial to use low concentrations of the filler, provided that their amount is large enough to give favorable properties to the composite. These results emphasize the importance of inspecting materials both at the nanoscale and the microscale.

Raman Microscopy. Representative Raman images created by the plotting of the intensity of the characteristic peak of $CaCO_3$ are shown in Figure 5. The images were measured from

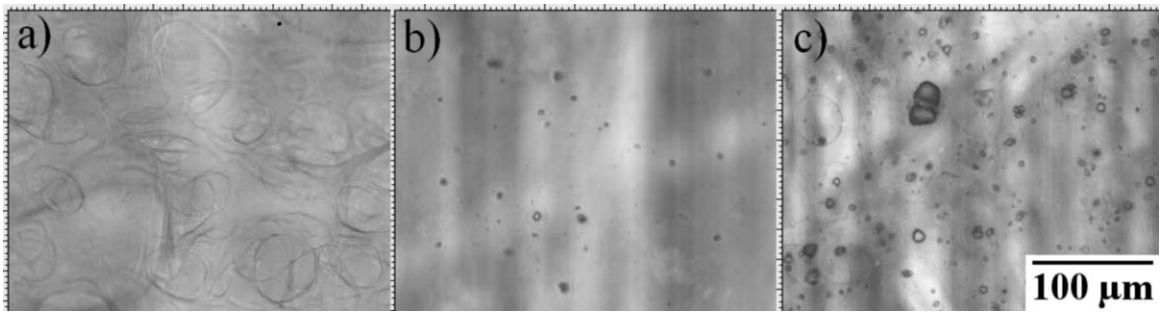

Figure 3. Optical microscopy images of the (a) PP and (b) 1.8 and (c) 8.1 wt % nano-$CaCO_3$/PP composites.

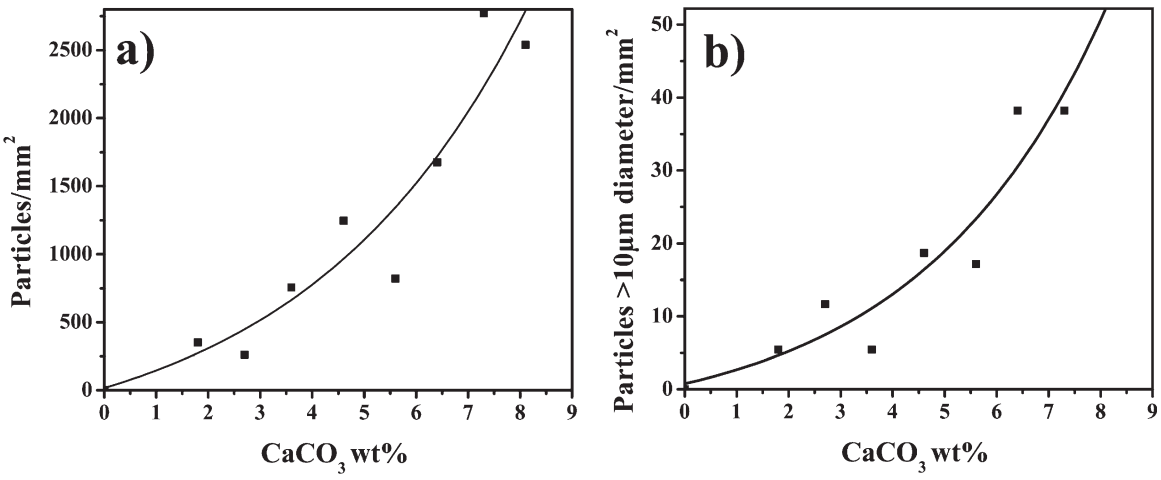

Figure 4. (a) $CaCO_3$ microparticle density and (b) density of large (>10 μm) $CaCO_3$ microparticles in the oriented composite films.

relatively large areas of 210 × 210 μm^2. Microparticles were observed as bright spots in several places in the images. It was important to note that the base level of the signal did not go to zero outside the particles, but it remained at a certain level. Closer inspection of the spectrum revealed that there was a small signal of $CaCO_3$ detectable everywhere in the sample. This signal originated from the averaged amount of a large number of nanoparticles in the focal volume. It was a direct measure of the average concentration of $CaCO_3$ distributed at the nanoscale. The stability of the base level throughout the whole

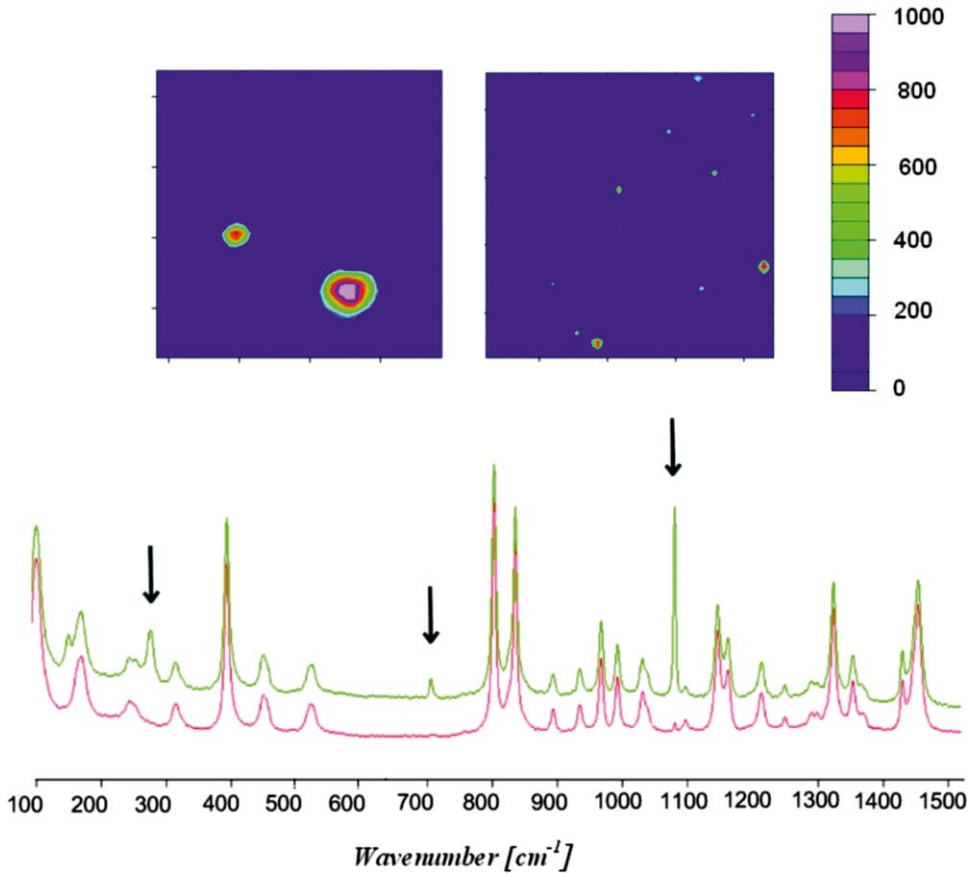

Figure 5. Raman contour plots and the spectra of 1.8 wt % nano-$CaCO_3$/PP composites. The characteristic peaks of $CaCO_3$ used for imaging are marked with arrows. The contour plots were generated by the integration of the intensity of the strongest peak. The upper green spectrum is from high-intensity region of the contour map, and the lower red spectrum is from the weak-intensity region. There was a signal from $CaCO_3$ even in the weak-intensity region. The area in the images is 210 × 210 μm^2, and the step size used was 3 μm. [Color figure can be viewed in the online issue, which is available at wileyonlinelibrary.com.]

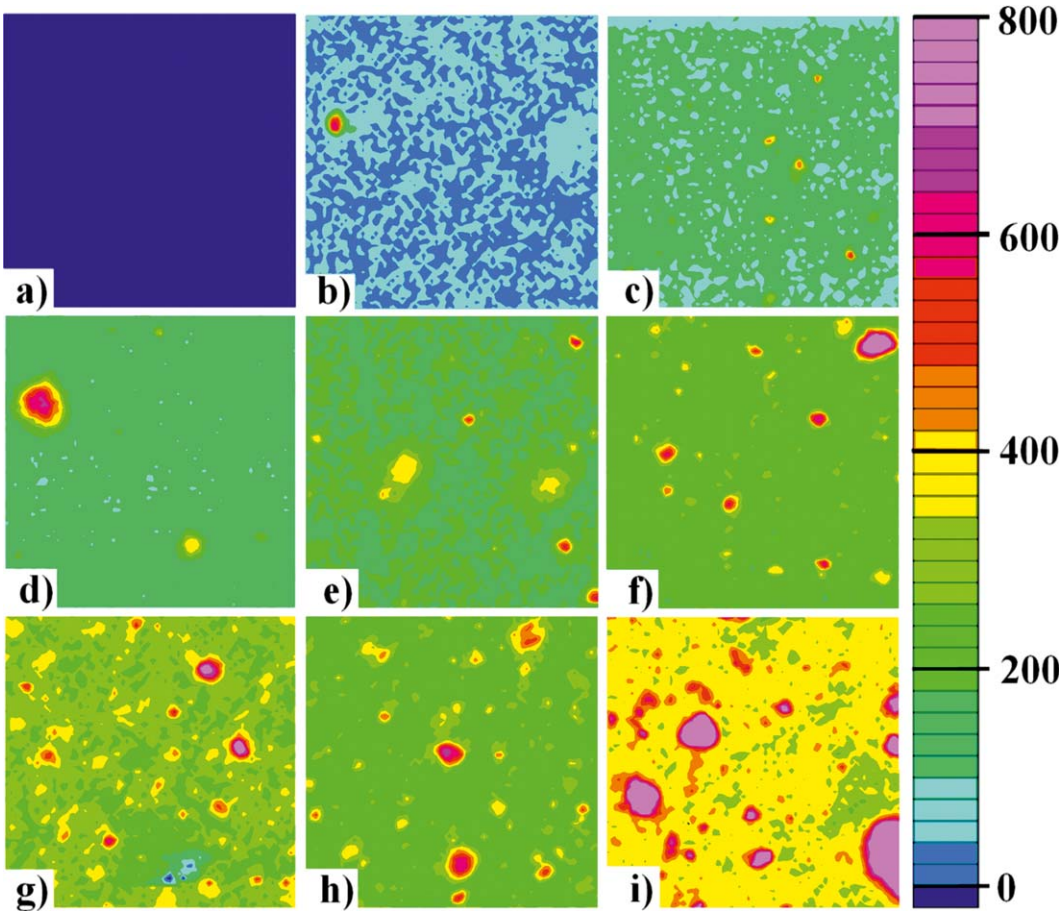

Figure 6. Raman contour maps (210 × 210 μm^2) of the cast samples generated by the integration of the most intense characteristic peak of $CaCO_3$: (a) pure PP and (b) 1.8, (c) 2.7, (d) 3.6, (e) 4.6, (f) 5.6, (g) 6.4, (h) 7.4, and (i) 8.1 wt % nano-$CaCO_3$/PP composite samples. The overall level of the $CaCO_3$ signal increased as the concentration of nano-$CaCO_3$ was increased in the composites. [Color figure can be viewed in the online issue, which is available at wileyonlinelibrary.com.]

sample indicated that the distribution of nanoparticles was homogeneous over the whole measured area. This result confirmed the picture of the sample morphology as a homogeneous nanodispersion of filler nanoparticles that was interrupted occasionally by very large particles. A representative image from every sample is shown in Figure 6. When comparing these contour plots, we observed that all of the composite samples contained large $CaCO_3$ agglomerates, and their amount and size increased with higher filler concentrations. The average base signal intensity level of $CaCO_3$ grew as the amount of nano-$CaCO_3$ was increased, but the level remained spatially stable within each sample. Thus, as shown by these examples, a Raman image revealed a great deal of information about the nanocomposites, including (1) the size and density of microparticles over a relatively large area, (2) the average concentration of the nanoparticles, and (3) the homogeneity of the nanoparticle distribution.

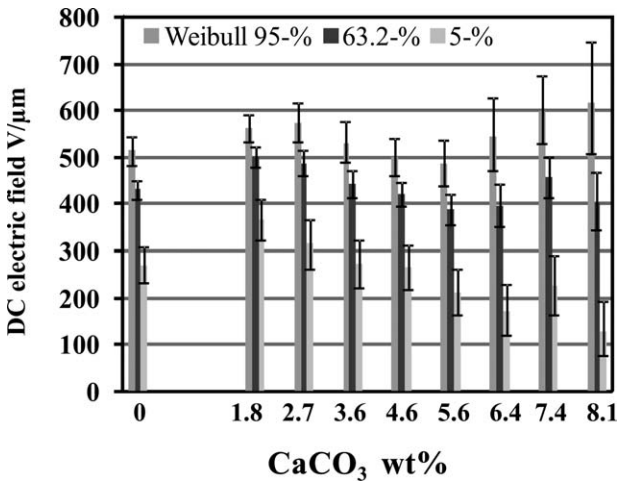

Figure 7. Dielectric breakdown strength of the oriented composite films represented by Weibull distributions with 95%, 63.2% (α), and 5% probabilities of breakdown at the respective electric field magnitude. The error bars show the 90% confidence intervals.

Dielectric Breakdown Strength

The Weibull distributed dc breakdown strength of the composite samples is shown in Figure 7. The shape of the distribution and deviation between parallel samples for each composite is represented by Weibull 95, 63.2 (α), and 5 percentiles, which correspond to the probability of breakdown at the respective electric field magnitude. Previously, it was found that small-area (<10 cm^2) Weibull α values for different industrial PP capacitor films varied between 450 and 850 V/μm dc, depending on the

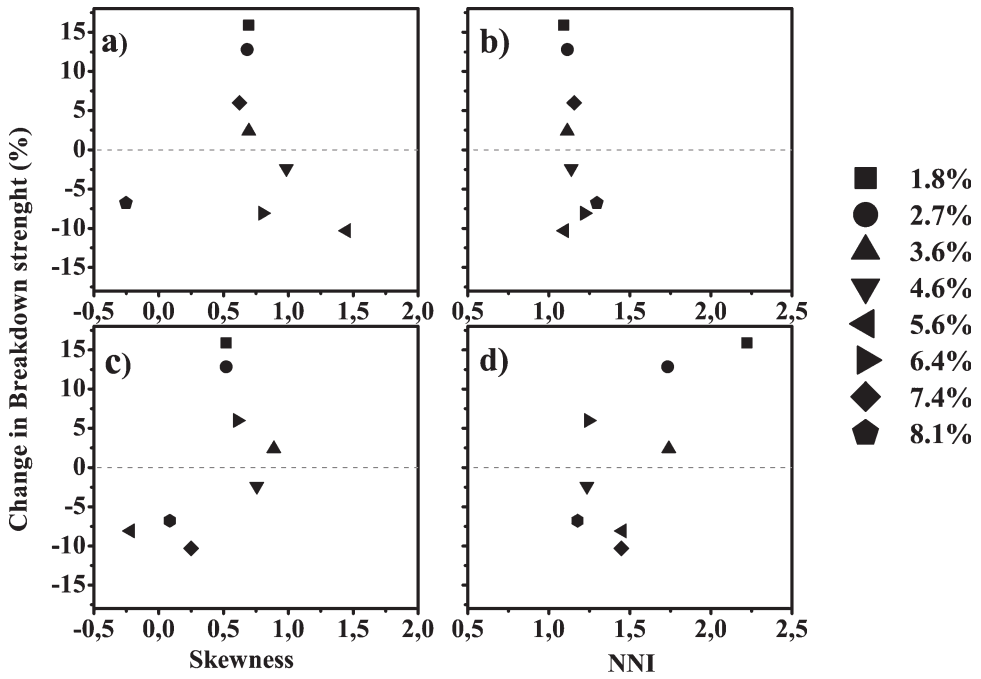

Figure 8. Relationship between the (a) skewness after the nanoparticles were counted in quadrats, (b) NNI of the nanoparticles, (c) skewness after the microparticles were counted in randomly distributed quadrats, and (d) NNI of the microparticles and with a 63.2% (α) breakdown strength of the oriented composite films. The symbol shows the amount of nano-$CaCO_3$ in the composite.

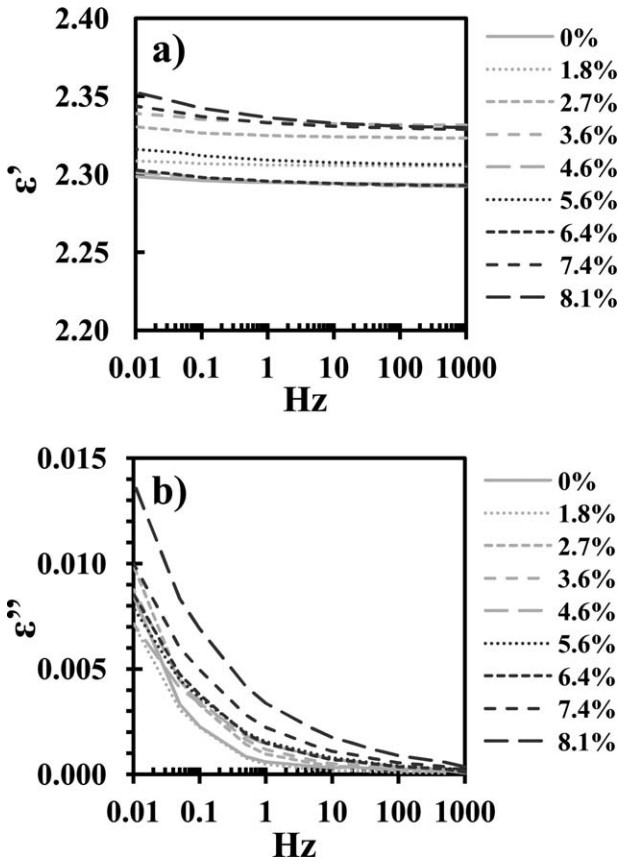

Figure 9. (a) ε' and (b) ε'' at different $CaCO_3$ contents as functions of the frequency.

grade of the film, and increased with a smaller electrode area.[21] The reference PP did not quite reach this level; this was also reflected in the performance of the composites. On the other hand, in the samples with the highest concentration of the filler material, the distribution indicated the presence of both very poor and good samples.

Overall, the composite with a 1.8 wt % nano-$CaCO_3$ content could stand the highest dc electric field; this was also slightly higher than the reference sample of pure PP. The trend of the breakdown strength was a decrease as the filler concentration was increased; meanwhile, the deviation between the parallel composite samples grew considerably. This growth of deviation was mainly caused by the appearance of lower individual breakdown results; this was possibly related to the increased amount of larger particles visible in the Raman images. Previously, it was reported that 4 and 7 wt % amounts of $CaCO_3$ in PP raised the breakdown strength under an ac electric field; this was explained by the fact that $CaCO_3$ composites could stand the high temperatures present at high fields much better than the pure PP.[12]

To establish the relationship between the dispersion quality and the dielectric breakdown strength, a 63.2%(α) breakdown strength of the oriented composite films was compared with the NNI and skewness of the distribution in Figure 8. It was reported previously that values greater than 0.7 for NNI and low absolute values of skewness (<1.5) were related to an improved dielectric breakdown strength.[17] The values of both NNI and skewness obtained for the studied materials were within these ranges. Thus, the quality of nanodispersion was not the main reason for changes in the breakdown strength

between the samples. In the literature, there are suggestions that nanoparticles might not dramatically increase the dielectric breakdown strength.[2] It should also be noted that in our case, the nanoparticles were not perfectly individually dispersed, but with agglomerates of 150 nm or greater, the interfacial effect between the particle and surrounding polymer was probably not optimal in these studied materials. However, the slight increase in the dielectric breakdown strength upon the addition of nanofiller indicated a favorable effect at relatively low concentrations. Because the quality of the nanodispersion remained good up to the highest concentrations, we believe that the decreasing trend in the breakdown strength at higher concentrations was due to the increase in the density of microparticles; this masked the expected favorable effect of increasing concentration of well-dispersed nanoparticles. This emphasizes the importance of multiscale structural characterization when one studies the effect of the concentration on the electric properties of composite materials. From a practical point of view, because of the presence of microparticles, the studied materials were hardly usable for capacitor applications.

Dielectric Spectroscopy

Figure 9 shows the frequency dependency of ε' and ε'', which represent polarization and losses, respectively, of the material in the electric field. The idea behind the measurement of ε', is that verified theories with properties at the molecular level exists, so it better represents the material properties as opposed to the dielectric breakdown strength, which also features the sample geometry. There were no major differences observed between the reference PP and the composites in ε', and the small changes in the overall level were within the variation seen between different samples of same material rather than correlated with the filler concentration. The slight increase in ε'' for the highest filler concentrations at low frequencies was probably due to the more abundant microparticles, which could have acted as an internal electric field distorting grain boundaries, where mobile charges could be trapped.

CONCLUSIONS

Studies of the multiscale structure and breakdown strength of PP doped with nano-$CaCO_3$ were carried out. We found that at doping levels of 1.8–8.1 wt %, the filler particles formed a homogeneous distribution of particles with diameters of greater than 150 nm; this was quantified by skewness and NNI analysis. At the same time, there was a smooth distribution of microparticles even at the lowest concentration, and their density increased exponentially with concentration. Raman microscopy was shown to be a particularly informative technique for revealing structural information at the nanoscale and microscale. Dielectric measurements indicated that the permittivity of the material was hardly affected by the incorporation of the filler. The dc breakdown strength increased slightly with 1.8 wt % of $CaCO_3$ but then decreases as a function of the concentration, largely because of the increase of low-field breakdowns, probably caused by the large microparticles present in the material. Thus, the positive effect of the nanodispersion was masked by the negative effect of the microparticles. The results point out the importance of multiscale structural analysis of composite samples in the study of concentration effects on the dielectric properties.

ACKNOWLEDGMENTS

One of the authors (S.V.) thanks Tuomas Turpeinen for his indispensable contributions to quantifying the particle dispersion. This research was funded by the Tekes Consortium's Functional Materials Programme projects NANOCOM and NANOPOWER.

REFERENCES

1. Lewis, T. *J. IEEE Trans. Dielectr. Electr. Insul.* **2004**, *11*, 739.
2. Tanaka, T.; Montanari, G.; Mulhaupt, R. *IEEE Trans. Dielectr. Electr. Insul.* **2004**, *11*, 763.
3. Frechette, M.; Trudeau, M.; Alamdari, H.; Boily, S. *IEEE Trans. Dielectr. Electr. Insul.* **2004**, *11*, 808.
4. Nelson, J. K.; Hu, Y.; Thiticharoenpong, J. *CEIDP* **2003**, 719.
5. Cao, Y.; Irwin, P.; Younsi, K. *IEEE Trans. Dielectr. Electr. Insul.* **2004**, *11*, 797.
6. Smith, R. C.; Liang, C.; Landry, M.; Nelson, J. K.; Schadler, L. S. *IEEE Trans. Dielectr. Electr. Insul.* **2008**, *15*, 187.
7. Roy, M.; Nelson, J.; MacCrone, R. K.; Schadler, L. S. *J. Mater. Sci.* **2007**, *42*, 3789.
8. Lu, J.; Wong, C. P. *I IEEE Trans. Dielectr. Electr. Insul.* **2008**, *15*, 1322.
9. Takala, M.; Ranta, H.; Nevalainen, P.; Pakonen, P.; Pelto, J.; Karttunen, M.; Virtanen, S.; Koivu, V.; Pettersson, M.; Sonerud, B.; Kannus, K. I. *IEEE Trans. Dielectr. Electr. Insul.* **2010**, *17*, 1259.
10. Zuiderduin, W.; Westzaan, C.; Huetink, J.; Gaymans, R. *Polymer* **2003**, *44*, 261.
11. Banghyi, G.; Karasz, F. E. *Colloid Polym. Sci.* **1987**, *265*, 394.
12. Takala, M.; Kortet, S.; Salovaara, P.; Karttunen, M.; Kannus, K. Presented at Nordic Insulation Symposium NORD-IS07, Lyngby, Denmark, June **2007**.
13. Garcia-Lopez, D.; Merino, J.; Pastor, J. *J. Appl. Polym. Sci.* **2003**, *88*, 947.
14. Wang, Y.; Lee, W. *Polym. Compos.* **2004**, *25*, 451.
15. Weon, J.; Gam, K.; Boo, W.; Sue, H.; Chan, C. *J. Appl. Polym. Sci.* **2006**, *99*, 3070.
16. Eteläaho, P.; Haveri, S.; Järvelä, R. *Polym. Compos.* **2011**, *32*, 464.
17. Calebrese, C.; Hui, L.; Schadler, L. S.; Nelson, J. K. *IEEE Trans. Dielectr. Electr. Insul.* **2011**, *18*, 938.
18. Kim, D.; Lee, J. S.; Barry, C. M. F.; Mead, J. L. *Microsc. Res. Tech.* **2007**, *70*, 539.
19. IEC/IEEE Guide for the Statistical Analysis of Electrical Insulation Breakdown Data (Adoption of IEEE Standard 930–2004); IEC Standard 625392007; International Electrotechnical Commission: Geneva, Switzerland, **2007**.
20. Recommended Methods for the Determination of the Permittivity and Dielectric Dissipation Factor of Electrical Insulating Materials at Power, Audio and Radio Frequencies Including Metre Wavelengths; IEC Standard 60250; International Electrotechnical Commission: Geneva, Switzerland, **1969**.
21. Laihonen, S. J.; Gäfvert, U.; Schütte, T.; Gedde, U. W. IEEE Trans. Dielectr. Electr. Insul. **2007**, *14*, 275.